Pergamon

Int. J. Heat Mass Transfer. Vol. 40, No. 10, pp. 2445–2460, 1997

0017–9310/97 $17.00+0.00

PII: S0017-9310(96)00288-8

Hydrodynamics and heat transfer in wavy annular gas–liquid flow: a computational fluid dynamics study

S. JAYANTI† and G. F. HEWITT

Department of Chemical Engineering, Imperial College, London SW7 2BY, U.K.

(*Received* 21 *March* 1995 *and in final form* 15 *July* 1996)

Abstract—Computational fluid dynamics techniques have been used to calculate the flow field and heat transfer through a wavy liquid film driven by gas shear. The geometry and flow conditions specified are typical of conditions encountered in gas–liquid annular flow. Results show that the flow in the substrate layer is laminar while that in the disturbance wave region is turbulent leading to a local enhancement of the transport coefficients. © 1997 Elsevier Science Ltd. All rights reserved.

1. INTRODUCTION

Annular two-phase flow occurs in steam generators and other heat exchangers over a wide range of flow conditions. The flow regime is characterised by the presence of a thin, wavy liquid film driven along the wall by the shear force exerted by the gas (or vapour) phase. Part of the liquid phase may also flow as droplets in the vapour core of the flow. In view of its importance, annular flow has received wide attention over the past four decades and a number of methods have been developed to predict the heat transfer coefficient in this flow regime. Apart from purely empirical correlations, analytical methods for calculating the evaporative heat transfer coefficient have also been presented (see [1–3], for example). In these models, the evaporative (non-bubbling) heat transfer through a thin, turbulent liquid film is considered. The heat flux through the liquid film is given by

$$\dot{q} = -(k_L + \rho_L C_{pL} \nu_h)\frac{dT}{dy}. \tag{1}$$

Here, $\dot{q}$ is the heat flux, C_{pL}, ρ_L and k_L are the specific heat, density and thermal conductivity, respectively, of the liquid, ν_h the turbulent thermal diffusivity and T the temperature at a distance y from the wall. If the film thickness is very small compared to the pipe diameter, as is usually the case in annular flow, then the heat flux through the film is constant and is equal to the wall heat flux, $\dot{q}_w$, and equation (1) can be rewritten in non-dimensional form as

$$\left(\frac{1}{Pr_L} + \frac{\nu_h}{\nu_L}\right)\frac{dT^+}{dy^+} = 1 \tag{2}$$

where the non-dimensional variables are defined as

$$T^+ = \frac{\rho L C_{pL} u^*(T_w - T)}{\dot{q}_w} \tag{3a}$$

$$y^+ = \frac{y u^*}{\nu_L} \tag{3b}$$

$$u^* = \sqrt{\frac{\tau_w}{\rho_L}}. \tag{3c}$$

Here, Pr_L is the liquid Prandtl number, ν_L the kinematic viscosity of the liquid, u^* the friction velocity, T_w the wall temperature and τ_w the average shear stress across the film. Integrating equation (2) from the wall to the interface, we get

$$T_i^+ = \int_0^{\delta^+}\left(\frac{1}{Pr_L} + \frac{\nu_h}{\nu_L}\right)dy^+ \tag{4}$$

where T_i^+ is the non-dimensionalised temperature at the interface and δ the film thickness, and the convective heat transfer coefficient, α_c, is given by

$$\alpha_c = \frac{\rho_L C_{pL} u^*}{T_i^+}. \tag{5}$$

Thus, if the variation of the turbulent thermal diffusivity, ν_h, across the film is known, then a relation can be obtained between the heat transfer coefficient, the film thickness (or the film flow rate) and the shear stress. It is usual to assume that the turbulent thermal diffusivity is the same as the turbulent eddy diffusivity of momentum (ν_m) for which many expressions are available. For example, Dukler [1] and Hewitt [2] used the eddy diffusivity expression of Diessler for $y^+ < 20$ and that of von Karman for $y^+ > 20$:

$$\nu_h = \nu_m = n^2 u y\left[1 - \exp\left(1 - \frac{\rho_L n^2 u y}{\nu_L}\right)\right] \qquad y^+ < 20 \tag{6a}$$

† Current address: Department of Chemical Engineering, Indian Institute of Technology, Madras 600036, India.

NOMENCLATURE

C_p	specific heat at constant pressure
$c_1, c_2 \ldots$	constants in turbulence modelling
D	tube diameter
f	friction factor
k	thermal conductivity
k	turbulent kinetic energy
k_s	equivalent sand grain roughness height
p	pressure
Pr	Prandtl number
$\dot{q}$	heat flux
Re	Reynolds number
t	time
T	temperature
u	velocity component
u^*	friction velocity
U	average velocity
U	time-average velocity
x_i	distance along the ith coordinate direction
y	normal distance from the wall.

Greek symbols

α	convective heat transfer coefficient
δ	film thickness
ε	turbulent energy dissipation rate
κ	von Karman constant
μ	dynamic viscosity
ν	kinematic viscosity or diffusivity
ρ	density
σ	constant in turbulence modelling
τ	shear stress.

Superscripts

+	non-dimensional quantity
′	fluctuating component
−	time-averaged quantity (overbar).

Subscripts

d	pertaining to disturbance wave
f	film
G	gas phase
h	thermal
i	interface
$i,j \ldots$	direction index
L	liquid phase
m	momentum
r	ripple
s	substrate
t	turbulent
w	wall.

$$\nu_h = \nu_m = \kappa \frac{(du/dy)^3}{(d^2u/dy^2)^2} \qquad y^+ < 20 \qquad (6b)$$

where n and κ are constants with values of 0.1 and 0.4, respectively. A simpler expression for ν_m, obtained from the so-called universal velocity profile, is used by Kosky and Staub [3] among others:

$$\nu_m = 0 \quad y^+ < 5 \qquad (7a)$$

$$\nu_m = \nu_L\left(\frac{y^+}{5} - 1\right) \quad 5 < y^+ < 30 \qquad (7b)$$

$$\nu_m = \nu_L\left(\frac{2y^+}{5} - 1\right) \quad y^+ > 30. \qquad (7c)$$

These expressions, when introduced into equations (4) and integrated give the dimensionless interface temperature, T_i^+:

$$T_i^+ = \delta^+ Pr_L \quad \delta^+ < 5 \qquad (8a)$$

$$T_i^+ = 5[Pr_L + \ln\{1 + Pr_L(\delta^+/5 - 1)\}] \quad 5 < \delta^+ < 30 \qquad (8b)$$

$$T_i^+ = 5[Pr_L + \ln\{1 + 5Pr_L\} + 0.5\ln(\delta^+/30)] \quad \delta^+ > 30 \qquad (8c)$$

which when substituted into equation (5) give the evaporative heat transfer coefficient. The dimensionless film thickness, δ^+, in the above expressions is related explicitly to Re_f, the film Reynolds number, defined as $4u_f\delta/\nu_L$ where u_f is the average film velocity, by curve-fitting the calculated variation:

$$\delta^+ = 0.7071 Re_f^{0.5} \quad Re_f < 50 \qquad (9a)$$

$$\delta^+ = 0.6323 Re_f^{0.5286} \quad 50 < Re_f < 1483 \qquad (9b)$$

$$\delta^+ = 0.0504 Re_f^{0.875} \quad Re_f > 1483. \qquad (9c)$$

This approach, although widely used, tends to overpredict the heat transfer coefficient [4] and suffers from many limitations. Perhaps the most serious of these are that

(i) The analysis is done for the mean film thickness and no explicit account is taken of the interfacial waves. There are two types of interfacial waves in vertical annular flow [5]: ripple waves which are small-amplitude, short-lived waves and disturbance waves which are long-wavelength, axially as well as circumferentially coherent waves. Although the omission of ripple waves in the analysis may lead to small errors, it is thought that the disturbance waves have an important effect on the transport properties in annular flow, and the omission of these may lead to large errors.

(ii) In the analysis, the flow is assumed to be turbulent and the turbulent thermal diffusivity is specified using empirical expressions which show a discontinuity at $y^+ = 30$. However, the liquid film in annular flow consists of a substrate layer of a relatively small thickness and a disturbance wave of a much larger thickness (of up to maybe five times the substrate film thickness). Since disturbance waves are formed above a film Reynolds number of about 300–500, it is possible that the flow in the substrate film is laminar and that in the disturbance wave is turbulent.

Both these shortcomings can be redressed by the use of computational fluid dynamics (CFD) techniques to calculate the flow field. In this approach, the governing (partial differential) equations of motion (representing, for example, the conservation of momentum and mass together with the appropriate boundary conditions and turbulence models) are reduced to a coupled set of algebraic equations using finite difference approximations at a number of grid points representing the flow domain. The algebraic equations are then solved iteratively using efficient numerical algorithms to give the flow field at the selected grid points (see, for example, [6, 7]). Over the past decade or so, these techniques have become quite popular and are now available in the form of computer codes incorporating well-established solution algorithms and turbulence and other physical models which can be used to investigate a wide variety of flows.

Application of CFD codes to the present problem enables one to obtain a flow field which satisfies a more fundamental set of equations describing the fluid flow and therefore is less arbitrary than the approach described by equations (1)–(9). Also, sophisticated turbulence models can be used to represent with fewer approximations the turbulence characteristics in the liquid film and specific account of the interfacial waves can be taken into account by including these in the flow domain. In the present paper, the application of the CFDS-FLOW3D computer code developed by AEA Technology, Harwell, England [8, 9] to investigate the hydrodynamics of the liquid film flow in annular flow is described. The problem formulation and details of the numerical methods are described in Section 2. The results of the calculations are discussed in Section 3 and the conclusions drawn from the study are reported in Section 4.

2. MATHEMATICAL MODELS AND NUMERICAL METHODS

2.1. *Problem formulation*

The flow situation considered here is shown schematically in Fig. 1. It consists of a liquid film bounded on one side by a wall and on the opposite side by a gas–liquid interface which is partly parallel to the wall (representing the substrate film) and partly wavy (representing a disturbance wave). The flow is from the left to the right (against the gravity vector which is shown in the figure) and the left and the right planes on the boundary are taken to be periodic planes representing the periodicity of the disturbance waves. The wall moves at the wave velocity in a direction opposite to the flow so as to keep the interface shape fixed, thus permitting a steady state calculation of the flow field. (Calculations of this type have previously given good results for the case of laminar, falling film waves [10]). The flow is driven by the shear stress imposed at the interface. The dimensions and flow conditions specified are typical of those occurring in annular flow.

It should be noted that since the film thickness is very small compared to the pipe radius, and since the flow is axisymmetric in vertical annular flow, the flow is formulated as two-dimensional, and a cartesian coordinate system is used instead of cylindrical (polar) coordinates. The profile of the interface is assumed (and is kept fixed throughout the calculations) and is typical of an interface having a disturbance wave in vertical annular flow [11]. As far as the fluid flow and turbulence are concerned, both the gas–liquid interface and the wall are treated alike, and no specific account is taken of turbulence suppression of damping at the former. While there is much debate and speculation as to whether or not suppression occurs, direct experimental evidence is hard to come by. Recent results from direct numerical simulation (DNS) studies of turbulence in stratified gas–liquid flow (see, for example [12, 13]) indicate that for high values of shear rate, the qualitative features of turbulence structure are alike at solid walls and at gas–liquid interfaces at the same shear rate. Thus, as far as the present calculations are concerned, no distinction is made between the liquid–solid interface and the liquid–gas interface as far as turbulence damping is concerned. The flow field and the temperature field in the flow domain are calculated using the CFDS-FLOW3D computer code. Details of the calculations are given below.

2.2. *Governing equations and turbulence models*

The flow of a fluid can be described mathematically in terms of a set of partial differential equations describing the conservation of mass, momentum and energy, and a set of boundary conditions for each variable. For incompressible, isothermal flow in a channel, the continuity and the momentum equations take the following form:

Continuity

$$\frac{\partial u_i}{\partial x_i} = 0. \tag{10}$$

Momentum conservation

$$\frac{\partial u_i}{\partial t} + u_j \frac{\partial u_i}{\partial x_j} = -\frac{1}{\rho}\frac{\partial p}{\partial x_i} + \nu \frac{\partial^2 u_i}{\partial x_j \partial x_j} \tag{11}$$

where u_i is the velocity component in the ith coordinate direction, p is the pressure, ν is the kinematic

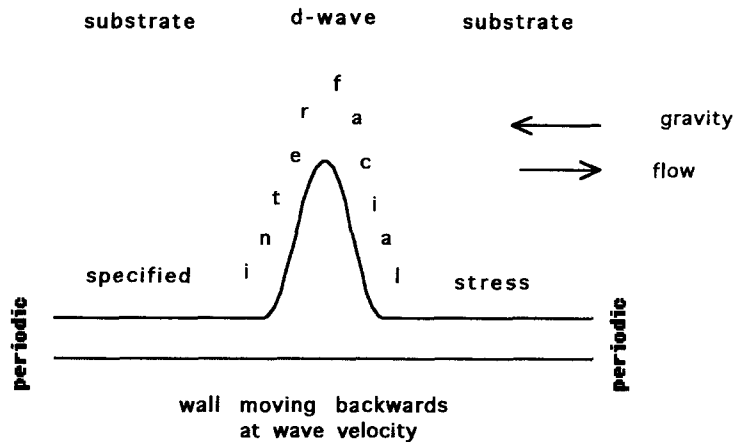

Fig. 1. Flow domain and boundary conditions. The direction of flow and of the gravity vector are as shown.

viscosity. The solution of these equations gives the instantaneous flow field for both laminar as well as turbulent flows. Such direct numerical simulation of turbulence is possible (see for example, [14]) but even for low Reynolds number flows in simple geometries requires huge computational effort. In practice, equations (10) and (11) are time-averaged and a turbulence closure model is used to represent the final (Reynolds stress) term in the time-averaged equation (13) below. Several types of closure models are available [15, 16], but those best suited for CFD calculations are the so-called phenomenological models in which transport equations are written in a form similar to the momentum transport equation (equation (2)) for variables representing the turbulent nature of the flow. Several types of phenomenological turbulence models of varying sophistication exist in the literature (see [15] for a review); here, we use two fairly standard models: (i) the standard k–ε model, and (ii) the low Reynolds number k–ε model. The details of these models are given below.

2.3. *The standard k–ε turbulence model*

Setting $u_i = U_i + u_i'$ etc. where U_i is the time-averaged quantity and u_i' is the fluctuating component, the time-averaged continuity and momentum equations can be written as

Continuity

$$\frac{\partial U_i}{\partial x_i} = 0. \tag{12}$$

Momentum conservation

$$\frac{\partial U_i}{\partial t} + U_j \frac{\partial U_i}{\partial x_j} = -\frac{1}{\rho}\frac{\partial P}{\partial x_i} + \frac{\partial}{\partial x_j}\left(\nu \frac{\partial U_i}{\partial x_j} - \overline{u_i' u_j'}\right). \tag{13}$$

The term $\overline{u_i' u_j'}$ appearing on the right-hand side is due to turbulent motion and is called the Reynolds stress tensor. It acts to promote the diffusion of momentum. This term is unknown and cannot be obtained by further time-averaging alone, and therefore has to be modelled. In the k–ε model, the turbulent motion is characterised by two quantities: k, the turbulent kinetic energy, defined as sum of the normal stresses, i.e. $k = \frac{1}{2}(\overline{u_i' u_i'})$, and ε the turbulent energy dissipation rate, defined as

$$\varepsilon = -\nu \overline{\frac{\partial u_i'}{\partial x_j}\frac{\partial u_j'}{\partial x_i}}.$$

The Reynolds stress term is expressed as being proportional to the symmetric part of the mean velocity gradient tensor. The function of proportionality is called the turbulent (eddy) viscosity, μ_t, and is related to k and ε. Thus,

$$\overline{u_i' u_j'} = -\nu_t\left(\frac{\partial U_i}{\partial x_j} + \frac{\partial U_j}{\partial x_i}\right) \tag{14}$$

$$\mu_t = \rho \nu_t = \rho c_\mu \frac{k^2}{\varepsilon}. \tag{15}$$

Two equations for the two extra unknowns, k and ε, can be derived exactly from first principles. However, these contain more unknown terms, and two transport equations of the type

$$\text{Advection} = \text{Production} - \text{Diffusion} - \text{Dissipation} \tag{16}$$

are solved for k and ε. The modelling equations that are actually solved are as follows:
Transport equation for k:

$$\frac{\partial k}{\partial t} + \frac{\partial (U_j k)}{\partial x_j} = \nu_t\left(\frac{\partial U_i}{\partial x_j} + \frac{\partial U_j}{\partial x_i}\right)\frac{\partial U_i}{\partial x_j} + \frac{\partial}{\partial x_j}\left(\frac{\nu_t}{\sigma_k}\frac{\partial k}{\partial x_j}\right) - \varepsilon. \tag{17}$$

Table 1. Constants used in the standard k–ε model

c_μ	c_1	c_2	σ_k	σ_ε
0.09	1.44	1.92	1.0	1.217

Transport equation for ε

$$\frac{\partial \varepsilon}{\partial t}+\frac{\partial(U_j\varepsilon)}{\partial x_j}=c_1\frac{\varepsilon}{k}\nu_t\left(\frac{\partial U_i}{\partial x_j}+\frac{\partial U_j}{\partial x_i}\right)\frac{\partial U_i}{\partial x_j}+\frac{\partial}{\partial x_j}\left(\frac{\nu_t}{\sigma_\varepsilon}\frac{\partial \varepsilon}{\partial x_j}\right)-c_2\frac{\varepsilon^2}{k}. \quad (18)$$

The constants in equations (17) and (18) are rather researcher-specific, but are close to those used in the present study which are given in Table 1.

2.4. *The low Reynolds number k–ε model*

The standard k–ε model described above has been developed for fully developed turbulent flow and is valid only at high Reynolds numbers. Since the turbulent fluctuations are damped near a solid wall, there will be a region close to the wall where viscous effects are important. In this region, the local turbulence Reynolds number, defined [17] as $Re_t=\rho k^2/\mu\varepsilon$, will be small and the high Reynolds number models are no longer applicable. For this reason, the standard k–ε model cannot be used to calculate the flow right up to the wall through the viscous sublayer. Use is made therefore of empirical laws of sufficient generality (such as the universal velocity profile) to connect the wall conditions such as shear stress and heat flux to the dependent variables just outside the viscous layer [15]. This "wall function" approach is however not always satisfactory, and in such cases, the low Reynolds number k–ε model, proposed initially by Jones and Launder [17] can be used. In this model two of the empirical constants used in the original k–ε model (namely, c_μ and c_2 in equations (15) and (18), respectively) are expressed [18] as functions of the turbulence Reynolds number, Re_t, which allows positional variation of these constants taking account, for example, of damping of turbulence very close to the wall and is, therefore, more realistic. The relevant functions are:

$$\mu_t=\rho\nu_t=\rho c'_\mu\frac{k^2}{\varepsilon} \quad (19)$$

where

$$c'_\mu=c_\mu\exp\left(-3.4\Big/\left(1+\frac{Re_t}{50}\right)^2\right) \quad (20)$$

and

$$c'_2=c_2[1-0.3\exp(-Re_t^2)]. \quad (21)$$

Two extra terms, one each in the k-equation and the ε-equation, are added to account for the variation of the kinetic energy and the dissipation rate in the viscous sublayer. The final equations for k and ε are given below

Transport equation for k at low Reynolds numbers

$$\frac{\partial k}{\partial t}+\frac{\partial(U_jk)}{\partial x_j}=\nu_t\left(\frac{\partial U_i}{\partial x_j}+\frac{\partial U_j}{\partial x_i}\right)\frac{\partial U_i}{\partial x_j}+\frac{\partial}{\partial x_j}\left[\left(\nu+\frac{\nu_t}{\sigma_k}\right)\frac{\partial k}{\partial x_j}\right]-\varepsilon-2\nu\left(\frac{\partial k^{1/2}}{\partial x_j}\frac{\partial k^{1/2}}{\partial x_j}\right). \quad (22)$$

Transport equation for ε at low Reynolds numbers

$$\frac{\partial \varepsilon}{\partial t}+\frac{\partial(U_j\varepsilon)}{\partial x_j}=c_1\frac{\varepsilon}{k}\nu_t\left(\frac{\partial U_i}{\partial x_j}+\frac{\partial U_j}{\partial x_i}\right)\frac{\partial U_i}{\partial x_j}+\frac{\partial}{\partial x_j}\left[\left(\nu+\frac{\nu_t}{\sigma_\varepsilon}\right)\frac{\partial \varepsilon}{\partial x_j}\right]-c'_2\frac{\varepsilon^2}{k}+2\nu\nu_t\left(\frac{\partial^2 U_i}{\partial x_j\partial x_j}\right)^2. \quad (23)$$

The constants used in this model are the same as those in Table 1 except for the above modifications. It should be noted that the modified constants tend towards those in the standard k–ε as the turbulent Reynolds number increases. In this model, it is not necessary to invoke any wall functions.

As mentioned earlier, no specific account of turbulence suppression or enhancement at the gas–liquid interface is taken in the present calculation. It is assumed that the turbulence characteristics near the wall and the interface vary alike. In the case of the low Reynolds number k–ε model, where the calculations proceed right up to $y^+=0$, where y is the normal distance from the wall, both the turbulence quantities go to zero at both the liquid–solid boundary and the liquid–gas boundary.

2.5. *Flow domain and boundary conditions*

The flow domain for the problem is shown schematically in Fig. 1. One-fifth of the interface length is covered by a disturbance wave, the rest being part of the substrate film. The height of the disturbance wave is five times the height of the substrate film (h_s), which itself is a small fraction of a millimetre. Because of foreshortening, the wave slope appears to be very steep; however, the average slope is only about 3–5°. These dimensions are typical of the liquid film in annular flow.

The boundary conditions are also shown in Fig. 1. The two inlet and outlet planes are periodic. At the interface, a shear stress in the flow direction is imposed. This interfacial shear stress changes with position. In the substrate section of the interface, it is taken to be equal to that for a liquid film in annular flow without disturbance waves. The interfacial shear stress in this region ($\tau_{i,r}$) is calculated as

$$\tau_{i,r}=\frac{1}{2}f_{i,r}\rho_G U_G^2 \quad (24)$$

where ρ_G and U_G are the density and the superficial velocity of the gas phase and $f_{i,r}$ is the interfacial friction factor in the ripple region given by the following expression

$$\frac{f_{i,r}}{f_G} = 0.856 + 0.00281 Re_G \frac{\delta_s}{D} \quad (25)$$

where δ_s is the substrate film thickness, D the tube diameter and Re_G the gas Reynolds number based on D and U_G and f_G is the gas phase friction factor based on Re_G . Equation (25) is a curve fit of the data of Shearer and Nedderman [19] for annular flow in the ripples-only regime.

In the disturbance wave region, the interfacial shear stress is calculated as

$$\tau_{i,d} = \frac{1}{2} f_{i,d} \rho_G U_G^2 \quad (26)$$

where the $f_{i,d}$, the interfacial friction factor in the disturbance wave region is given by an explicit version [20] of the Colebrook–White formula:

$$f_{i,d} = \left[-3.6 \log_{10} \left\{ \frac{6.9}{Re_G} + \left(\frac{k_{s,d}}{3.7D} \right)^{1.11} \right\} \right]^{-2}. \quad (27)$$

Here, $k_{s,d}$ is the equivalent sand roughness which is taken to be five times the local film thickness and thus is the highest at the peak of the wave. This specification of the interfacial roughness appears rather arbitrary; however, two factors have been taken into account in developing this prescription.

(i) It is known that the equivalent sand roughness of the liquid film in annular flow is roughly five times the mean film thickness (see for example, [21]) as far as the interfacial friction is concerned.

(ii) Recent high-speed photographic pictures of disturbance waves in annular flow [22, 23] show that although the disturbance wave, on a time-averaged basis, is a gentle variation of the film thickness (with an average wave slope of 3–5°), there are large scale perturbations on the wave surface itself which appear to have an amplitude of the order of the film thickness.

Taken together, these observations indicate that the shear stress varies along the wave surface and that it may be represented by a varying equivalent sand roughness which is roughly equal to five times the local film thickness. Indeed, this prescription gives the shear stress variation shown in Fig. 2, which is typical of annular flow [24]. The mean shear stress value (summed over the substrate and the disturbance wave region) is taken to be representative of the flow conditions in annular flow.

The boundary condition for the side wall is that it moves opposite to the flow direction at the wave velocity. This velocity is not known *a priori* but is such that the momentum balance on the overall flow domain is satisfied [10]. In the present case of upward annular flow with periodic boundary conditions, it is the velocity at which the interfacial shear force is balanced by the wall shear force and the gravitational force. Thus, the wave velocity is obtained by calculating the flow field and the wall shear stress for a specified wall velocity, and improving upon this guess using the force balance. This procedure, when repeated a number of times, should lead to convergence and thus to the true wave velocity.

2.5. *Details of numerical methods*

The calculations were done using the Rel.3.1.2 version of the CFDS-FLOW3D computer program developed by AEA Technology [9]. The code uses a finite difference (volume) methods on a general non-orthogonal body-fitted grid and has a polyalgorithmic structure whereby options are available for the user to select from different discretisation schemes, solution algorithms and physical models. It is based on a non-staggered grid method, and uses the Rhie–Chow algorithm [25] extended to three dimensions [26] to overcome the problem of chequerboard oscillations usually associated with the use of non-staggered grids. In the present calculations, the SIMPLEC algorithm [27] is used for pressure-velocity decoupling and the QUICK scheme [28] is used for the discretisation of the advection term in the momentum equations. More details of FLOW3D and the turbulence models can be obtained from Burns and Wilkes [26]. The results of the calculations are described below.

3. RESULTS OF CALCULATIONS

The methodology described in Section 2 was used to calculate the flow field under typical air–water annular flow conditions in 30 mm diameter tube. The results are discussed in here in two parts. Calculations describing the hydrodynamics of the flow are discussed in Section 3.1 and the implications on heat transfer are discussed in Section 3.2.

3.1. *Investigation of the hydrodynamics of the flow*

In these calculations, the flow conditions in a typical air–water annular flow experiments were considered [23]. The tube diameter and the substrate film thickness were taken to be 30 and 0.15 mm, respectively. The profile of the disturbance region was assumed to be sinusoidal with the maximum film thickness being five times the substrate thickness. The disturbance wave region was assumed to cover 20% of the total interfacial area. The length of the disturbance wave region was 20 mm; this was followed by a substrate film region of a length of 80 mm. Since the calculations were two-dimensional, this corresponded to the case of an axisymmetric wave. The film flow was assumed to be driven by air, with a density of 2.15 kg m^{-3}, flowing at a mean velocity of 50 m s^{-1}. The assumed interfacial shear stress resulting from this is shown in Fig. 2.

The problem is posed such that it is not known *a priori* whether or not the flow is turbulent. Indeed, it may be partly turbulent in the sense that the flow in

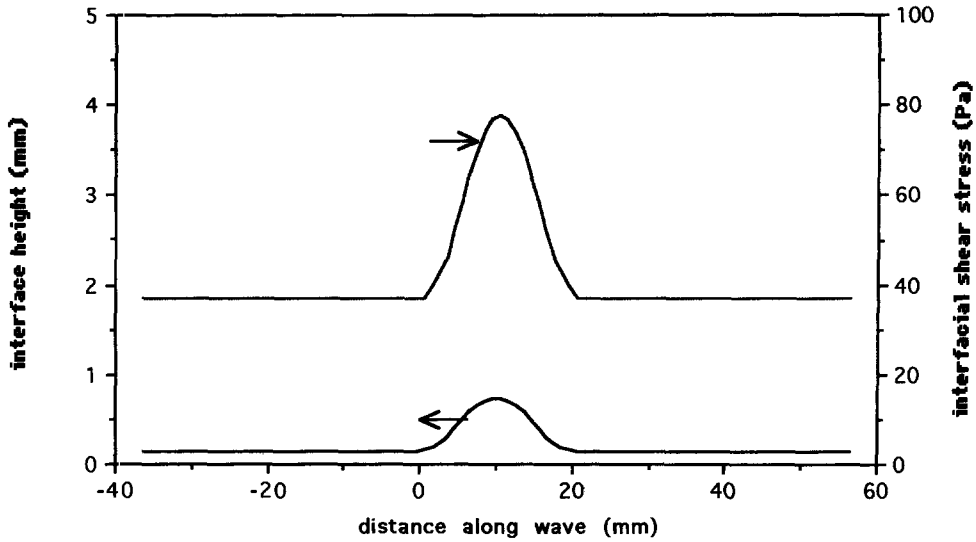

Fig. 2. Specified shear stress variation at the gas–liquid interface corresponding to a gas density of 2.15 kg m^{-3}, superficial gas velocity of 75 m s^{-1} in a tube of 30 mm diameter.

the substrate region may be laminar and that in the disturbance wave region turbulent. In view of this, calculations have been done to investigate all the possibilities. Thus, Case I assumes laminar flow in the entire flow domain and the laminar flow equations (Section 2.2) are solved. In Case II, turbulent flow is assumed, and the standard k–ε turbulence closure model (see Section 2.3) is used to represent the turbulence effects. In Case III, the low Reynolds number k–ε turbulence closure model (see Section 2.4) is used; this allows for partial or complete relaminarisation of flow under certain conditions. All the calculations were done on a 48 × 30 body-fitted grid with 48 grid nodes in the flow direction and 30 nodes in the film height direction. The results are described below.

The velocity field calculated in Case I (laminar flow) is shown in Fig. 3(a). For the sake of clarity, the velocity vectors at only some points are drawn and the actual grid is much finer than that shown in the figure. The vectors are drawn in a coordinate frame moving with the wave, and thus, the wall moves from the right to the left at the wave velocity, predicted in this case to be 2.6 ms^{-1}. The effect of gas shear at the interface is in the opposite direction and the flow conditions are such that the substrate interface moves faster than the wave. This is evidenced by an interfacial velocity from left to right in the substrate. The increased interfacial shear in the disturbance wave region gives rise to a higher interfacial velocity here, and a strong recirculation pattern is set up under the wave. This can be clearly seen in the streamfunction plot shown in Fig. 3(b) where the recirculation "bubble" extends right down to the bottom wall.

If the flow is assumed to be fully turbulent everywhere in the film, the picture one gets is quite different. The velocity vectors and the corresponding streamfunction contours calculated in Case II using the standard k–ε model are shown in Fig. 4(a,b), respectively. In this case, a slightly higher wave velocity (of 2.65 m s^{-1}) is predicted. However, due to high effective viscosity of the flow, the interface velocity in the substrate film is less than the wave velocity, and all the vectors in the substrate region are from right to left. It is only in the disturbance wave region (where the interfacial shear stress is much higher) that the interface velocity is higher than the wave velocity. The streamfunction contours show that the recirculation bubble is confined in this case to the top half of the disturbance wave region.

The velocity vectors and the streamfunction contours obtained from Case III using the low Reynolds number k–ε model are shown in Fig. 5(a,b), respectively. It can be seen here that the results appear to be a combination of the two cases considered above. The flow in the substrate is similar to that in the substrate film in Case I in the sense that the interface velocity is much higher than that of the wave, predicted in this case to be 3.05 m/s. However, in the disturbance wave region, the velocity field resembles that in Case II in that the velocity profiles here do not shown any inflection point. Thus, the flow field predicted by the low Reynolds number k–ε model exhibits laminar and turbulent characteristics. This can be seen very clearly in the contour plots of the effective viscosity (sum of laminar viscosity of the fluid and eddy viscosity, if any) and turbulent kinetic energy shown in Fig. 6(a,b), respectively. These are obtained using the low Reynolds number k–ε model. In the case of laminar flow, the viscosity would be constant throughout the flow domain and the turbulent kinetic energy would be zero everywhere. However in Fig. 6(a), there is a significant variation of the effective viscosity in the disturbance wave region whereas outside it, it is nearly constant. The contour values show that in the disturbance wave region, the effective viscosity is many times higher than that of laminar viscosity whereas

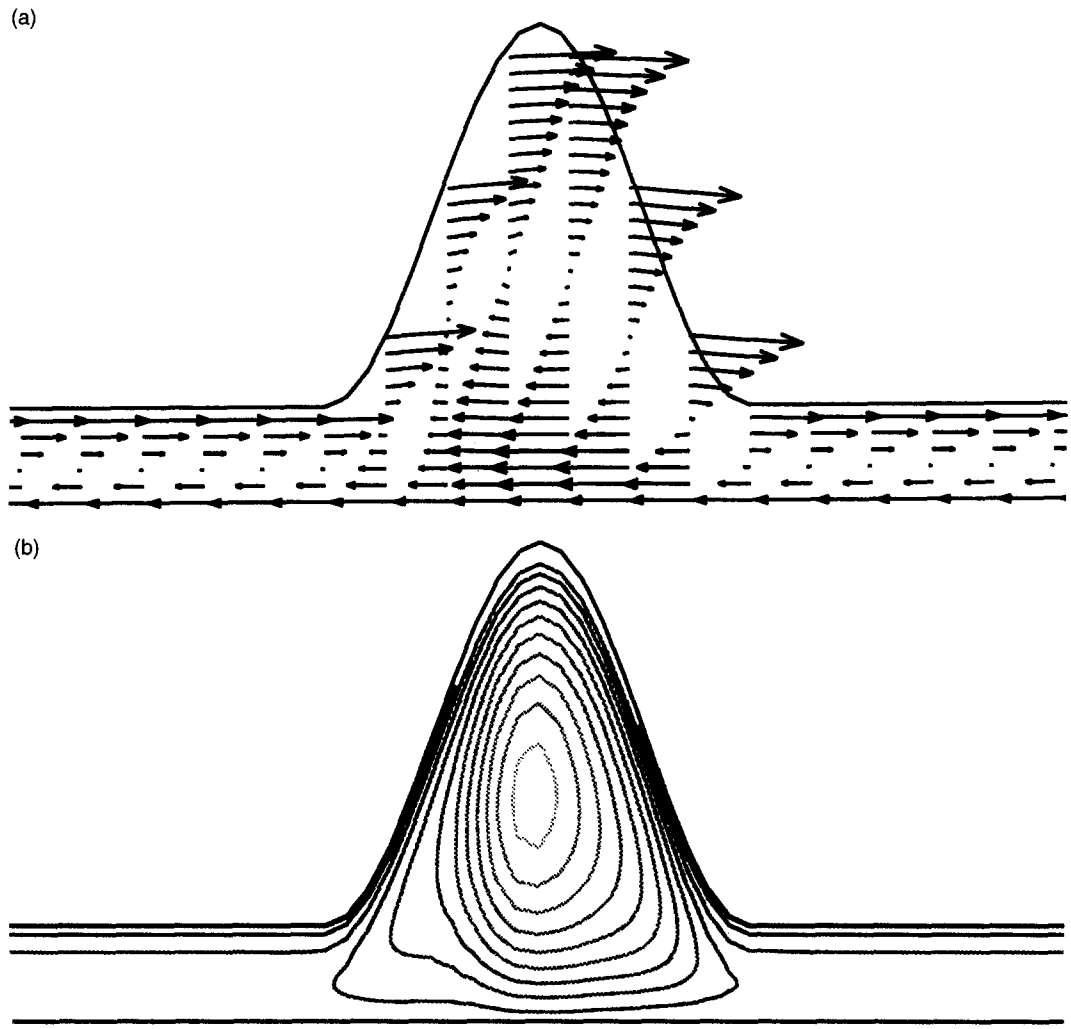

Fig. 3. (a) Velocity vectors; and (b) streamfunction contours obtained from Case I with laminar flow assumption. Wall moves from right to left at 2.6 m s^{-1} in the direction of the gravity vector.

the two are equal in the substrate region. Similarly the turbulent kinetic energy is zero in the substrate region and is non-zero in the disturbance wave region. Thus, the low Reynolds number k–ε model predicts that the flow is laminar in the substrate region and turbulent in the disturbance wave region. However, when the standard (high Reynolds number) k–ε model is used, the predicted effective viscosity and turbulent kinetic energy values (Fig. 7(a,b), respectively) indicate that the flow is turbulent everywhere.

Thus, application of different models gives different results, and other criteria must be used to determine which of them is the most accurate. For this purpose, the wall shear stress variation predicted by each model is compared in Fig. 8 with the wave profile and the interfacial shear stress (which is specified as a boundary condition). Note that although the length-averaged wall shear stress is the same for all the models (since each flow field satisfies the momentum balance on the flow domain), the variation along the wave can be different, and this may provide some indication as to the accuracy of the prediction. Figure 8(a) for the Case I (laminar flow) shows that the wall shear stress in the substrate region is much higher than the interfacial shear stress, and that it is much lower and, indeed, becomes negative, in the disturbance wave region. This is contrary to what is expected; simultaneous measurement of film thickness and wall shear stress [24, 29] show that the wall shear stress is higher in the disturbance wave region. This means that the fully laminar assumption of Case I is incorrect.

The predictions of the standard k-ε model (Fig. 8(b)) and of the low Reynolds number k–ε model (Fig. 8(c)) show a wall shear variation similar to that found in experiments, namely, that it is significantly higher in the disturbance wave region. Both predict a substrate region shear stress which is roughly equal to the interfacial shear stress which is again consistent with a thin film assumption [5]. The major difference between the two predictions is that in the former, the substrate film is taken to be turbulent, whereas the low Reynolds number k–ε model suggests that it is

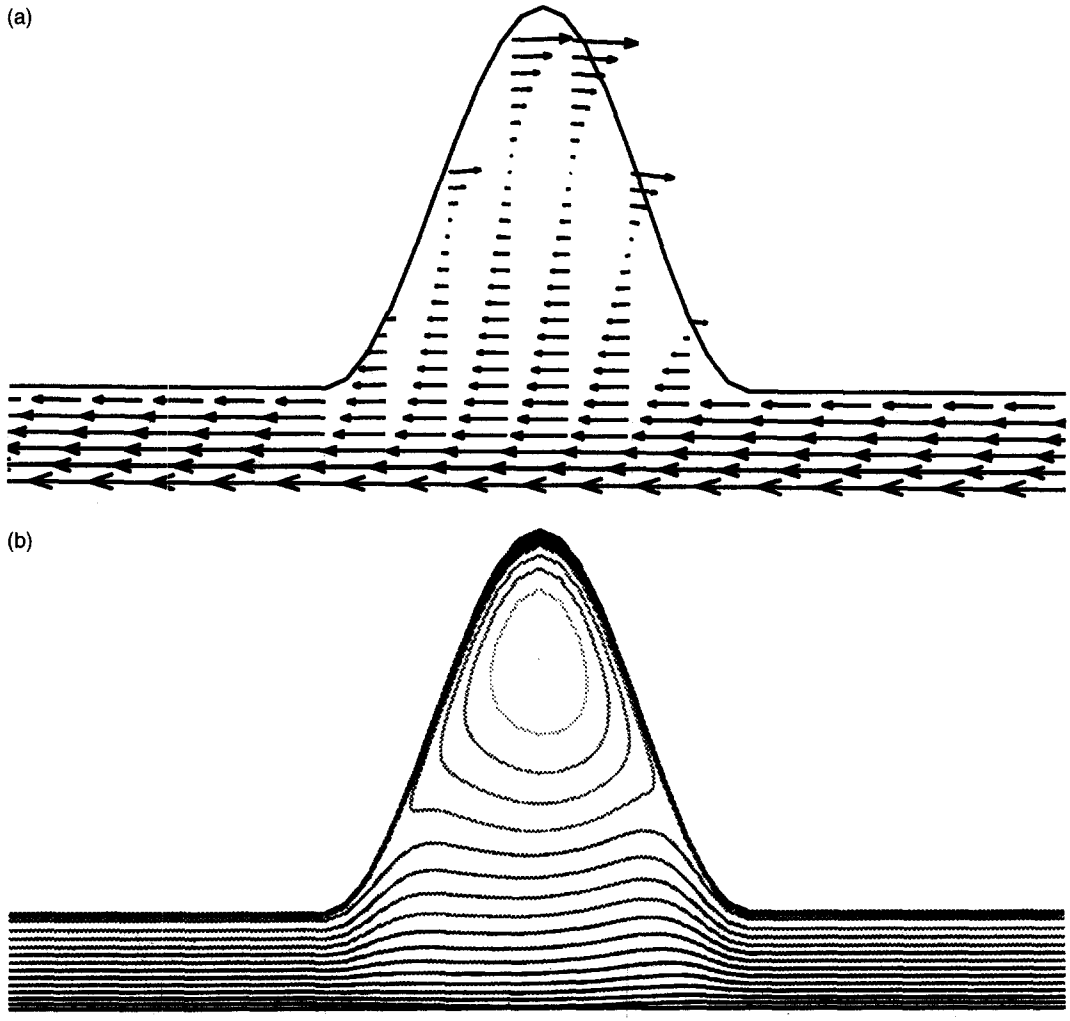

Fig. 4. (a) Velocity vectors; and (b) streamfunction contours obtained from Case II using the standard k–ε turbulence model. Wall moves from right to left at 2.65 m s^{-1}.

laminar. While this leads to only a small difference in the wall shear stress predictions of the two models, in the case of the heat transfer coefficient, the predictions are quite different both in magnitude and in trend. The predicted local heat transfer coefficient (defined as the wall heat flux divided by the temperature difference between the wall and the interface) is compared in Fig. 9 for a fluid of Prandtl number of one with a constant wall heat flux boundary condition for the side wall and a constant temperature boundary condition at the interface. Here, the turbulent thermal diffusion assumed in the standard k–ε model and the thinness of the substrate film cause the heat transfer coefficient in this region to be very high, in fact, higher than that in the disturbance wave region, where, although the turbulent diffusivity is higher (Fig. 6(b)), the heat must be transported across a much thicker film. The low Reynolds number k–ε model, which predicts laminar flow in the substrate, gives a much lower heat transfer coefficient in the substrate, and the variation of the heat transfer coefficient is similar to that of the wall shear stress, i.e. higher in the disturbance wave region.

Thus, from a heat transfer point of view, it is important to determine which of the two turbulence models gives the more accurate prediction. This is done here by examining the applicability of the two models. As mentioned in Section 2.3, the standard k–ε model uses a wall function approach [17] to account for the no-slip boundary condition. Here, the universal velocity profile is used to estimate the values of velocity, k and ε at the first grid point from the wall; these are then used to calculate the values in the interior of the flow domain assuming the flow to be turbulent as modelled by the standard k–ε model. For good accuracy, this usually requires that the first grid from the wall is located such that

$$30 < y_1^+ < 100 \tag{28}$$

where y_1^+ is the dimensionless normal distance from the wall of the closest grid point. Due to this restric-

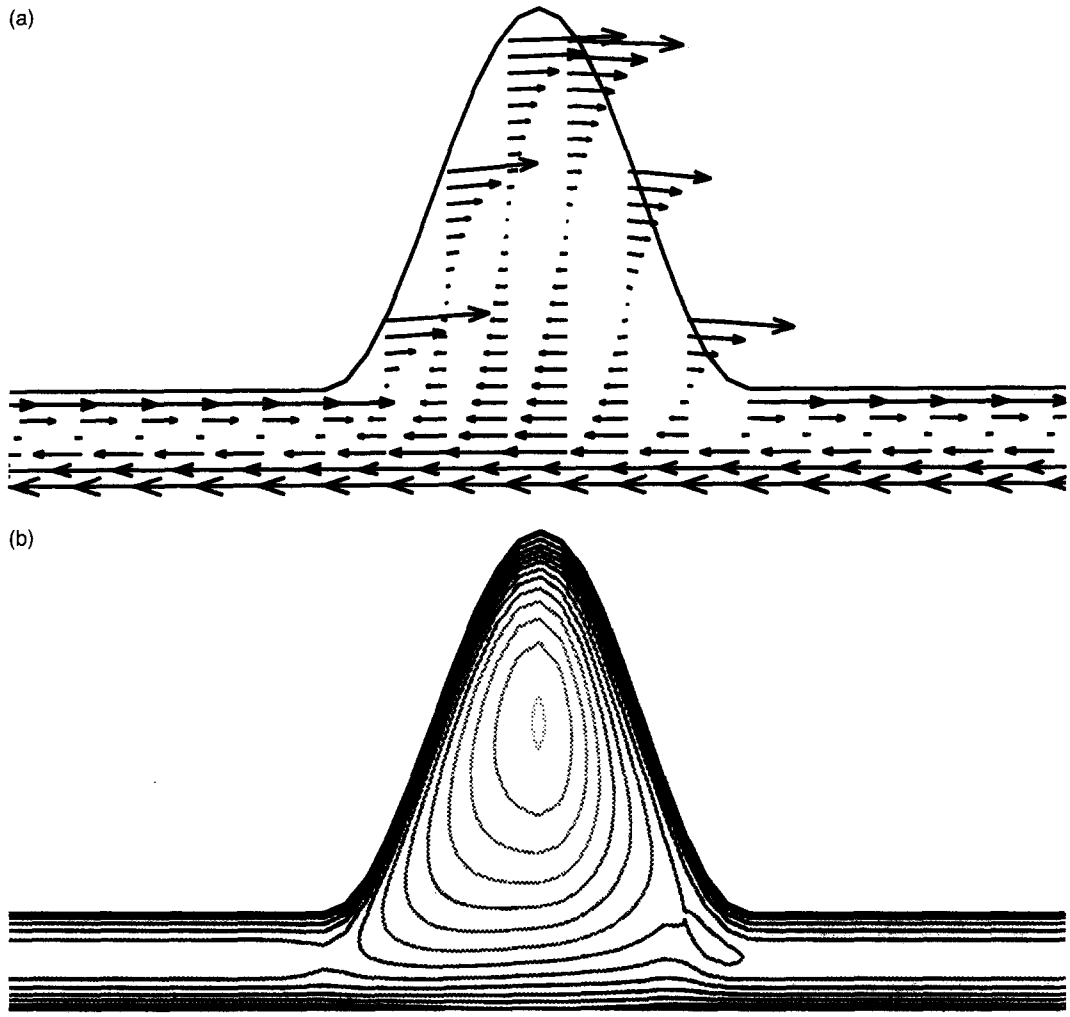

Fig. 5. (a) Velocity vectors; and (b) streamfunction contours obtained from Case III using the low Reynolds number k–ε turbulence model. Wall moves from right to left at 3.05 m s^{-1} in the direction of the gravity vector.

tion, this approach is well-suited for cases in which the flow near the wall is essentially parallel to the wall. Additionally, the flow Reynolds number must be sufficiently high so that y_1^+ satisfying equation (28) is still physically close to the wall so that imposition of the wall function does not have a dominant effect on the flow field in the rest of the flow domain.

When seen from this point of view, the standard k–ε model is found to be unsuitable for the present case, especially in the substrate region. Here the physical dimensions of the flow field are such that, assuming a constant shear across the film, the maximum distance from the wall, i.e. δ^+, is only 29. If this is divided into 30 intervals, then $y_1^+ = 1$ which does not satisfy the condition (28). If this condition were satisfied, it would then be equivalent to specifying the flow field in the whole of the flow domain. The condition (28), however, it not so restrictive in the disturbance wave region. At the peak, the interfacial shear stress is nearly two and a half times higher than in the substrate and the film thickness is five times higher; thus the maximum δ^+ is approximately 350.

Another way of looking at this is through the film Reynolds numbers. For a liquid film flowing due to interfacial shear, the substrate film Reynolds number can be estimated in the following way. Assuming that the flow field is the same as that for a thin, smooth, laminar film driven by a constant shear stress, the velocity profile in the film is given by

$$u = \frac{\tau}{\mu} y \tag{29}$$

and the film Reynolds number is then given by

$$Re_f = \frac{2\rho_L \tau_i \delta^2}{\mu^2}. \tag{30}$$

For Case I, the substrate film Reynolds number is

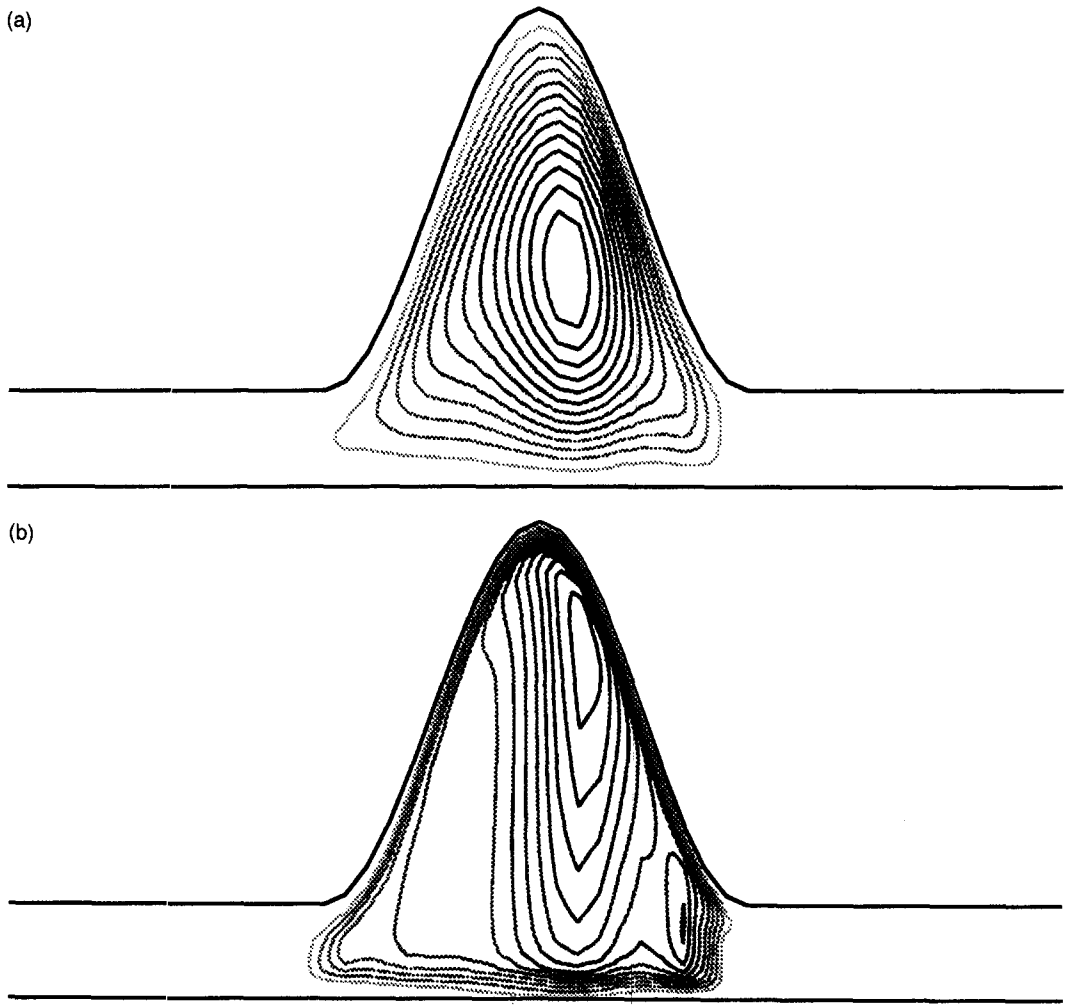

Fig. 6. Contour plots of: (a) effective viscosity (sum of molecular and eddy viscosities); and (b) turbulent kinetic energy obtained using the low Reynolds number k–ε model. The effective viscosity is equal to the molecular viscosity in the substrate and on the gas–liquid and the solid–liquid interfaces. The corresponding turbulent kinetic energy here, therefore, is zero. In both figures, the contours near the centre of the disturbance wave have the highest values.

therefore 1670. Since film flow becomes turbulent at a Reynolds number of about 1800 [30], the substrate film flow is either laminar or close to the transition. In either case, the standard (high Reynolds number) k–ε model cannot be applied. Indeed, the substrate film Reynolds number (obtained from the velocity field) predicted by this model is 620 which is much less than the expected value of 1670. In contrast, the low Reynolds number k–ε model predicts a value of 1680 which is close to the expected value. The lower value predicted by the former must be due to the assumption of turbulent flow in the film (increasing the frictional resistance and thus decreasing the flow rate and Re_f). At the peak of the disturbance wave region, the predicted values are 6980 and 9000 by the standard and the low Reynolds number k–ε models, respectively. Thus, the flow would clearly be turbulent here which explains the smaller difference between the predictions of the two models. It is interesting to note that the heat transfer coefficients predicted by the two models (Fig. 9) are much closer at the peak of the wave where turbulent diffusion is expected to be dominant whereas they differ greatly in the substrate region.

In view of the above discussion, we conclude that of the three models, the low Reynolds number k–ε model gives the most accurate results. The calculations also show that the substrate film is laminar and the disturbance wave region is turbulent. This picture is consistent with the study of Martin and Azzopardi [31] who conjectured that disturbance waves are created by turbulence bursts in the liquid film near the point of inception. They found that the frequency of turbulent bursts and of the disturbance waves showed quantitatively the same trend with dimensionless distance from the wall and with friction velocity. These results and those from the present calculations support the view that the disturbance waves act as packets of turbulence which are trans-

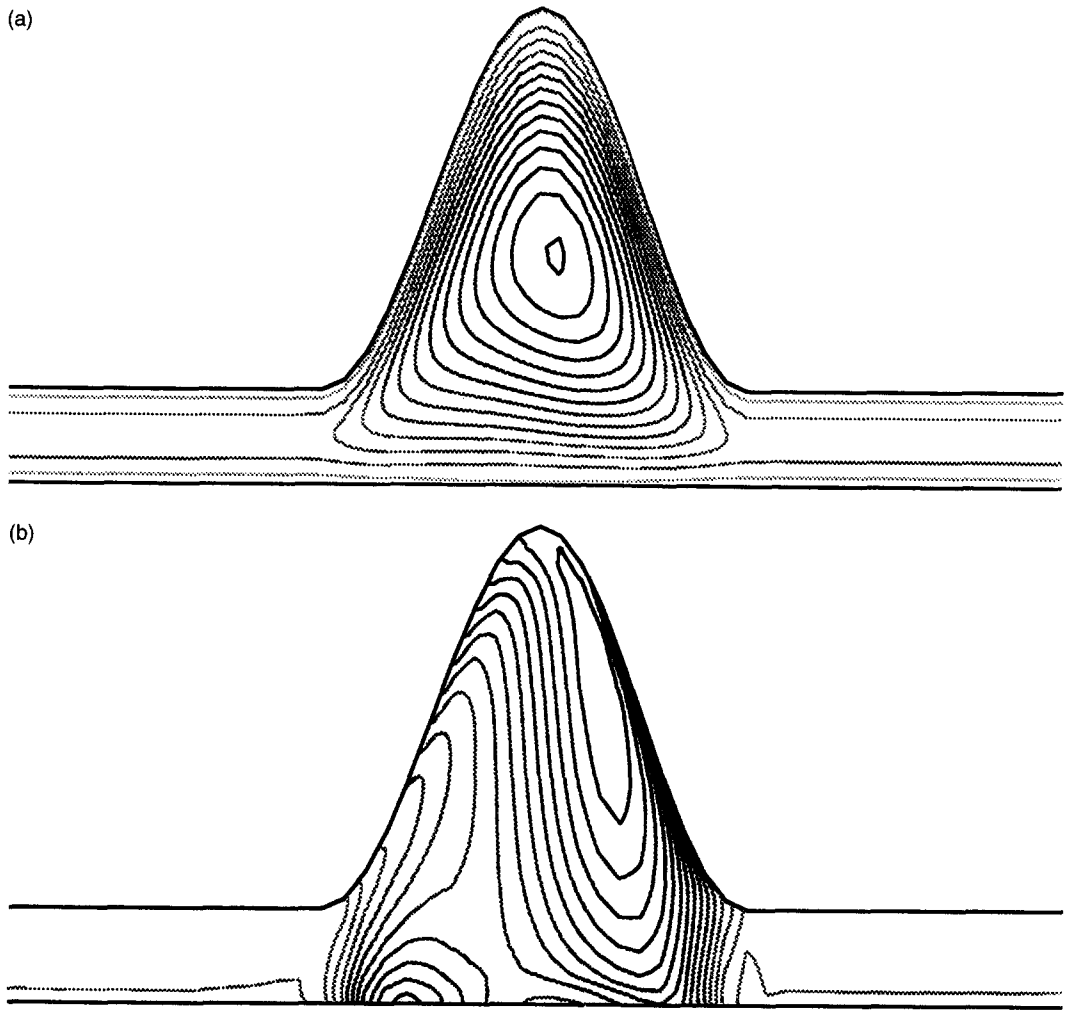

Fig. 7. Contour plots of: (a) effective viscosity (sum of molecular and eddy viscosities); and (b) turbulent kinetic energy obtained using the standard k–ε model. The contours near the centre of the disturbance wave have the highest values.

ported along the tube by the gas phase. The implications of this on heat transfer are studied in the next section.

3.2. *Heat transfer through the film*

As shown in Fig. 9 above, the heat transfer coefficient predicted by the low Reynolds number k–ε model varies with position and is significantly higher in the disturbance wave region in spite of the larger film thickness there. The thermal boundary conditions for this case represent non-bubbling evaporation at the interface. It would be interesting to compare the heat transfer coefficients predicted by the various methods. This is done in Fig. 10 for the case of a liquid having a thermal conductivity of 0.6 Wm K^{-1} and a specific heat of 4200 J kg^{-1}, corresponding to the properties of water at 20 C. In Fig. 10(a), the predictions of: (i) the laminar flow; (ii) the low Reynolds number k–ε model; (iii) the standard k–ε model; and (iv) the one-dimensional, flat interface analysis described in Section 1 are compared. The values from (i) and (ii) are much smaller than that from (iv) and are higher under the wave, although only by a small amount in (i). The higher value, in spite of there being a much thicker film in the wave, is perhaps due to the large recirculation bubble in the wave region (see Fig. 3(b). The predictions of (iii) are much higher than even that of (iv) which must be due to the fact that the model is not applicable in the substrate region, as explained in Section 3.1 above. The length-averaged values from the four methods are listed in Table 2, which again shows, in particular, that taking account of the waviness of the interface and the nature of the flow in the substrate and in the disturbance wave region results in a much smaller value of the heat transfer coefficient than that obtained from the one-dimensional analysis. This is consistent with the experimental findings of Aounallah *et al.* [4]. The variation of the Nusselt number along the wave predicted by the low Reynolds number k–ε model is shown in Fig.

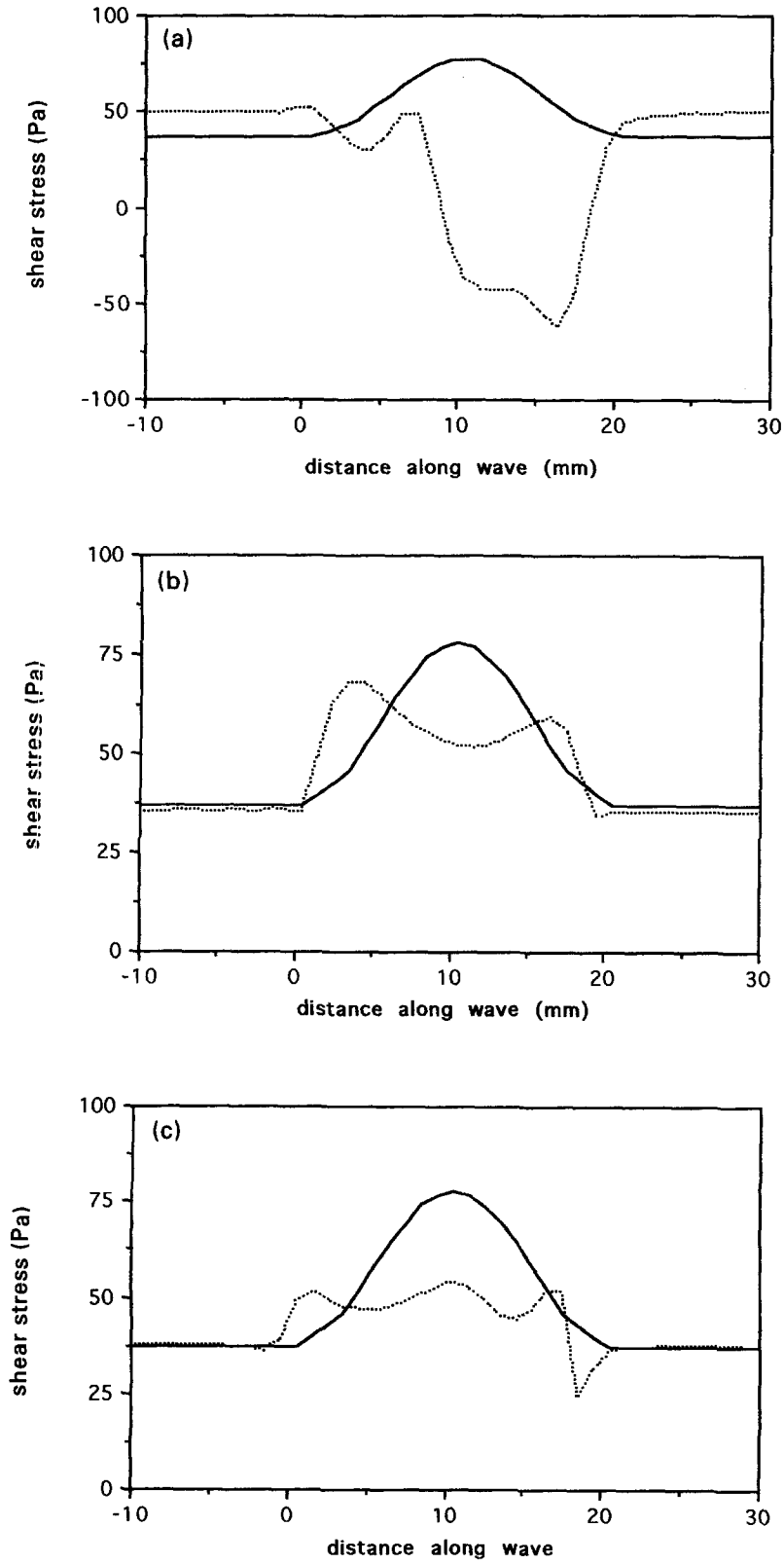

Fig. 8. Wall shear stress (dotted line) and interfacial shear stress (solid line) for: (a) Case I; (b) Case II; and (c) Case III.

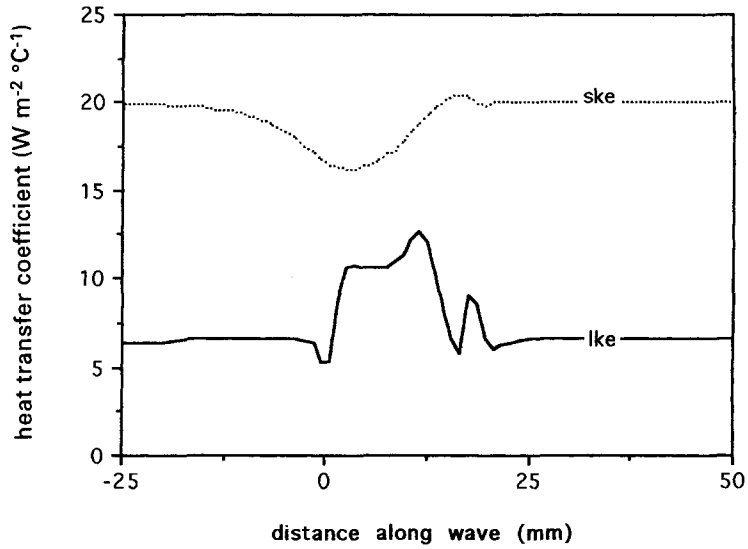

Fig. 9. Heat transfer coefficient variation predicted by the standard k–ε (ske) and the low Reynolds number k–ε (lke) model. Liquid Prandtl number = 1.

Table 2. Length-averaged heat transfer coefficient from various methods; properties of water at 20 C

Calculation method	Heat transfer coefficient ($Wm^{-2}K^{-1}$)
1-dim analysis with flat interface	15650
2-dim CFD: laminar flow	4505
2-dim CFD: standard k–ε model	37000
2-dim CFD: low Re k–ε model	6065

10(b). The fact that the local Nusselt number is much higher under the wave than in the laminar sublayer shows that disturbance waves enhance the local heat transfer coefficient. Comparing this with the enhancement produced in the laminar flow calculations (Fig. 10a(i)), it can be concluded that the enhancement under the disturbance waves is mainly due, not to the presence of a large recirculation area, but to the occurrence of turbulent flow.

4. CONCLUSIONS

Results obtained from the calculation of the flow field in the liquid film under typical annular flow conditions show that the flow in the substrate region is likely to be laminar while it is turbulent in the disturbance wave region. Because the turbulent diffusivity in the disturbance wave region is much higher than the molecular diffusivity, the heat transfer coefficient in this region is higher than that in the substrate region although the heat has to be transported through a much thicker film. Thus, disturbance waves in annular flow can be viewed as packets of turbulence which are transported along the tube by the gas phase and which lead to local enhancement of the transport coefficients.

Acknowledgements—S. Jayanti gratefully acknowledges the financial support received from the Science and Engineering Research Council for the work described in this report.

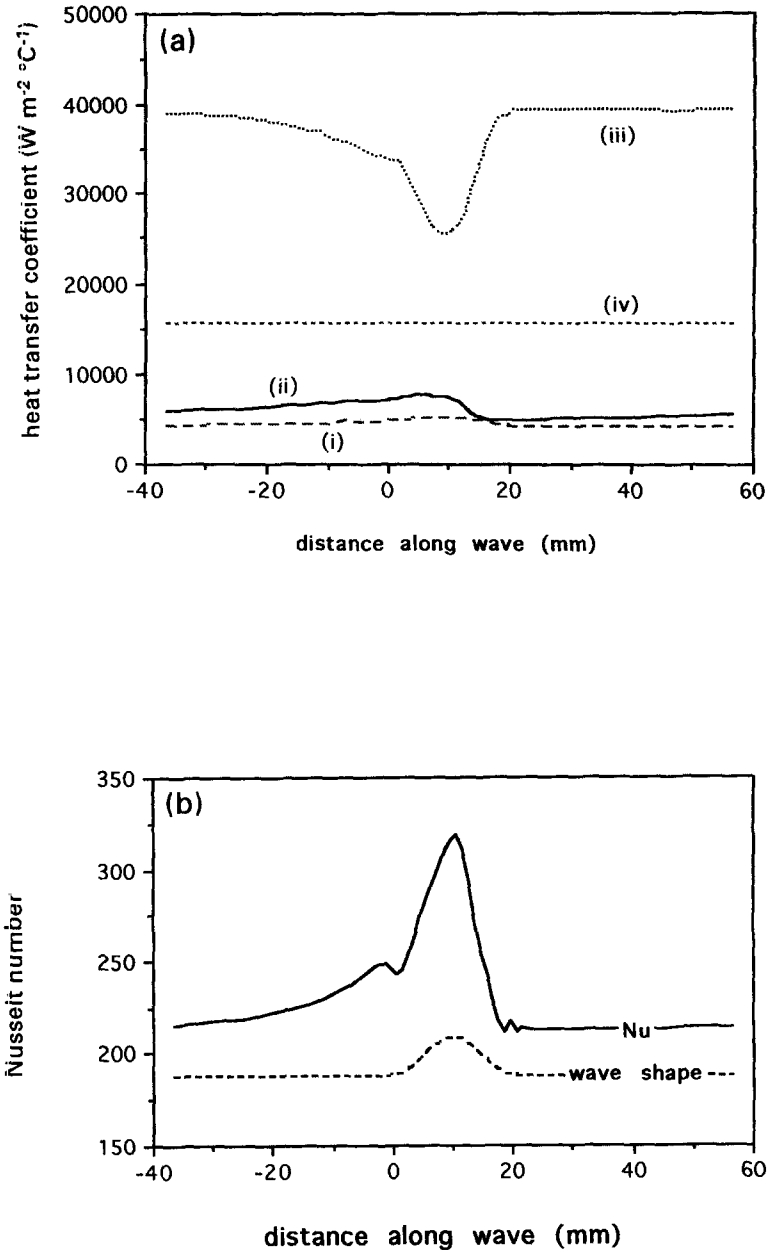

Fig. 10. (a) Comparison of the heat transfer coefficient predicted by various methods: (i) laminar flow; (ii) low Reynolds number k–ε model; (iii) standard k–ε model; and (iv) one-dimensional model; (b) Variation of the Nusselt number along the wave as predicted by the low Reynolds number k–ε model. Liquid Prandtl number = 7.

REFERENCES

1. Dukler, A. E., Fluid mechanics and heat transfer in falling film systems. *Chemical Engineering Progress Symposium Series*, 1960, **56(30)**, 1–10.
2. Hewitt, G. F., Analysis of annular two-phase flow: Application of the Dukler analysis to upward vertical flow in a tube. UKAEA Report no. AERE-R3680, 1961.
3. Kosky, P. G. and Staub, F. W., Local condensing heat transfer coefficients in annular flow regime. *AIChE Journal*, 1971, **17**, 1037–1043.
4. Aounallah, Y., Kenning, D. B. R., Whalley, P. B. and Hewitt, G. F., Boiling heat transfer in annular flow, Paper no. FB3. *Proceedings of 7th International Heat Transfer Conference*, Munich, Germany, 1982.
5. Hewitt, G. F. and Hall-Taylor, N. S., *Annular Two-phase Flow*. Pergamon Press, Oxford, 1970.
6. Roache, R. J., *Computational Fluid Dynamics*. Hermosa, Albuquerque, New Mexico, 1976.
7. Patankar, S. V., *Numerical Heat Transfer and Fluid Flow*. Hemisphere, Washington, D.C. 1980.
8. Jones, I. P., Kightley, J. R., Thompson, C. P. and Wilkes, N. S., FLOW3D a computer code for the prediction of laminar and turbulent flow and heat transfer. Release 1. UKAEA Report no. AERE R11825, 1985.
9. CFDS, FLOW3D Release 3.2.1: User Manual, Com-

putational Fluid Dynamics Services (CFDS), Harwell Laboratory, AEA Technology, Didcot, 1993.
10. Jayanti, S. and Hewitt, G. F., Hydrodynamics and heat transfer in laminar falling films. *International Journal of Heat Mass Transfer*, 1997, **40,** 179–190.
11. Hewitt, G. F., Disturbance waves in annular two-phase flow, paper 18. *Proceedings of Institution Mechanical Engineers* 1969-70, 1970, **184,** part 3c, pp.142–150.
12. Banerjee, S., Turbulence structure and transport mechanisms at interfaces, Vol. I, paper KN-26. *Proceedings of the 9th International Heat Transfer Conference*, Jerusalem, Israel, 1990, pp. 395–418.
13. Banerjee, S., Turbulence structures. *Chemical Engineering Science*, 1992, **47,** 1793–1817.
14. Moin, P. and Kim, J., Numerical investigation of turbulent channel flow. *Journal of Fluid Mechanics*, 1982, **118,** 341–378.
15. Rodi, W., Turbulence models and their application in hydraulics—a state of the art review. Presented by the IAHR section on Fundamentals and Division II: *Experimental and Mathematical Fluid Dynamics*, 2nd edn.
16. Lesieur, M., *Turbulence in Fluids*, Martinus Nijhoff, Dordrecht, Netherlands, 1986.
17. Jones, W. P. and Launder, B. E., The prediction of laminarization with a two-equation model of turbulence. *International Journal of Heat and Mass Transfer*, 1972, **15,** 301–314.
18. Launder, B. E. and Sharma, B. I., Application of the energy-dissipation model of turbulence to the calculation of flow near a spinning disc. *Letters in Heat and Mass Transfer*, 1974, **1,** 131–138.
19. Shearer, C. J. and Nedderman, R. M., Pressure gradient and liquid film thickness in co-current upwards flow of gas–liquid mixtures: application to film cooler design. *Chemical Engineering Science*, 1965, **20,** 671–683.
20. Haaland, S. E. Simple and explicit formulas for the friction factor in turbulent pipe flow. *ASME Journal of Fluids Engineering*, 1983, **105,** 89.
21. Owen, D. G., An experimental and theoretical analysis of equilibrium annular flows. Ph.D. thesis, University of London, 1986.
22. Hewitt. G. F., Jayanti, S. and Hope, C. B., Structure of thin liquid films in gas–liquid horizontal annular flow. *International Journal of Multiphase Flow*, 1990, **16,** 951–957.
23. Wolf, A., Jayanti, S. and Hewitt, G. F., On the nature of ephemeral waves in vertical annular flow. *International Journal of Multiphase Flow*, 1996, **22,** 325–333.
24. Govan, A. H., Hewitt, G. F., Owen, D. G. and Bott, T. R., Wall shear stress measurements in vertical air-water annular two-phase flow. *International Journal of Multiphase Flow*, 1989, **15,** 307–325.
25. Rhie, C. M. and Chow, W. L., Numerical study of the turbulent flow past an air foil with trailing edge separation. *AIAA Journal*, 1983, **21,** 1527–1532.
26. Burns, A. D. and Wilkes, N. S., A finite difference method for the computation of fluid flows in complex three-dimensional geometries. UKAEA Report no. AERE R12342, 1987.
27. van Doormaal, J. P. and Raithby, G. D., Enhancement of the SIMPLE method for predicting incompressible flows. Numerical Heat Transfer, 1984, **7,** 147–163.
28. Leonard, B. P., A stable and accurate convective modelling procedure based on quadratic upstream interpolation. *Computational Methods in Applied Mechanical Engineering*, 1979, **19,** 59–98.
29. Martin, C. J., Annular two-phase flow. Ph.D. thesis, University of Oxford, 1983.
30. Hewitt, G. F., Shires, G. L. and Bott, T. R., *Process Heat Transfer*. Begell House, CRC Press, New York, 1994.
31. Martin, C. J. and Azzopardi, B. J., Waves in vertical annular flow. *PhysicoChemical Hydrodynamics*, 1985, **6,** 257–265.